Study and Characterization of Zn-Bi_2O_3 Nanocomposite Using Theoretical and Experimental Method

Kalkidan Gemeda Manyahle

A Thesis Submitted to Department of Applied Physics
School of Applied Natural Science
Presented in Partial Fulfillment of the Requirement for the
Degree of Master's in Condensed Matter Physics

Office of Graduate studies
Adama Science and Technology University

June, 2024
Adama, Ethiopia

Study and Characterization of Zn-Bi_2O_3 Nanocomposite Using Theoretical and Experimental Method

Kalkidan Gemeda Manyahle

Advisor

Gashaw Beyene (Ph. D)

A Thesis Submitted to Department of Applied Physics

School of Applied Natural Science

Presented in Partial Fulfillment of the Requirement for the Degree of Master's in Condensed Matter Physics

Office of Graduate studies

Adama Science and Technology University

June, 2024

Adama, Ethiopia

Declaration

I hereby declare that this Master Thesis entitled "Study and Characterization of Zn-Bi_2O_3 Nanocomposite Using Theoretical and Experimental Method" is my original work. That is, it has not been submitted for the award of any academic degree, diploma or certificate in any other university. All sources of materials that are used for this thesis have been duly acknowledged through citation.

________________	________________	________________
Name of the student	Signature	Date

Recommendation of Advisor

I, the major advisor of this Thesis, hereby certify that we have read the revised version of the thesis entitled ''Study and Characterization of Zn-Bi_2O_3 Nanocomposite Using Theoretical and Experimental Method" prepared under our guidance by Kalkidan Gemeda submitted in partial fulfillment of the requirements for the degree of Master Science in Condensed Material Physics. Therefore, I recommend the submission of revised version of the thesis to the department following the application procedures.

________________	________________	________________
Major Advisor	Signature	Date
________________	________________	________________
Co-advisor	Signature	Date

Approval Page

I/we, the advisors of the thesis entitled “Study and Characterization of Zn-Bi_2O_3 Nanocomposite Using Theoretical and Experimental Methods “and developed by Kalkidan Gemeda Manyahle, hereby certify that the recommendation and suggestions made by the board of examiners are appropriately incorporated into the final version of the thesis.

Major Advisor	Signature	Date
Co-advisor	Signature	Date

We, the undersigned, members of the Board of Examiners of the thesis by Kalkidan Gemeda Manyahle have read and evaluated the thesis entitled “Study and Characterization of Zn-Bi_2O_3 Nanocomposite Using Theoretical and Experimental Method and examined the candidate during open defense. This is, therefore, to certify that the thesis is accepted for partial fulfillment of the requirement of the degree of Master of Science in condensed matter physics.

Chairperson	Signature	Date
Internal Examiner	Signature	Date
External Examiner	Signature	Date

Final approval and acceptance of the thesis is contingent upon submission of its final copy to the Office of Postgraduate Studies (OPGS) through the Department Graduate Council (DGC) and School Graduate Committee (SGC).

Department Head	Signature	Date
School Dean	Signature	Date
Office of Postgraduate Studies, Dean	Signature	Date

ACKNOWLEDEMENT

First, I would like to praise the almighty God that helps me to negotiate this work and his internal love and grace which enable me to succeed through my life. Next, I would like to admit the excellent guidance, stimulant and support of my thesis counsels Gashaw Beyene (Ph. D) throughout my thesis bid. It's only with their mentoring, leadership and cooperation that I was suitable to finish this thesis. I'm also thankful and offer my sincere thanks and gratefulness for his constant guidance and obliged to him for sparing his precious time. His unflagging trouble also deserves special citation than without whom the fulfillment of this entire work would have been insolvable. I would also like to thank my musketeers and classmates for their support, stimulant, and helpful discussion. Finally, I want to express my love and gratefulness to my cherished family for their understanding, support, and love throughout the duration of my studies.

Table of Content

Contents pages

List of Figures

List of Acronyms and Abbreviations

Bi = Bismuth

DF = Dielectric Function

NP = Nanoparticle

PL = Photoluminescence

SPR = Surface Plasmon Resonance

XRD = X-Ray diffraction

Zn $(NO3)_3$.5H_2O = Zinc Nitrate

Zn =Zinc

ZnO = Zinc Oxide

Abstract

Bi_2O_3 nanoparticle is the promising material for various applications because of its noble properties. In this study, we studied the properties of Bi_2O_3 based nanocomposite using experimental and theoretical method. We synthesized Bi_2O_3 based nanocomposite particle using biological and chemical synthesize technique. The synthesized nanoparticles were characterized using PL spectroscopy and XRD. From the characterization methods, we got the expected result. We also investigated theoretically the optical properties of Zn-Bi_2O_3 nanocomposites which embedded non-absorptive passive medium as a host matrix. The polarizability, refractive index, and optical absorbance of the composite nanostructures are investigated using the Maxwell-Garnet effective medium theory within the framework of the electrostatic approximation. The simulations were performed using the wolfram Mathematica software. We observe that two set of resonance peaks in the visible (above 300 nm) and visible-near infrared (between $450 - 600$ nm) spectral region for different values of metal fraction and filling factor. These two set of resonances are appeared almost at the same positions for all polarizability, refractive index, and optical absorbance. The effect of the permittivity of the medium, the size of the core, and the shell on the extinction spectrum and the refractive index were investigated.

CHAPTER ONE

Introduction

1.1 Background of the Study

In this work, we study synthesize and characterize Zn-$Bi_2O_{3,}$nanocomposite using theoretical and experimental methods. Nanocomposites have attracted significant attention due to their unique parcels arising from the combination of multiple element accoutrements at the nanoscale. Among these, Zn-$Bi_2O_{3,}$nanocomposites have shown pledge for colorful operations, including optoelectronics, photovoltaics, and photocatalysis, owing to their interesting optic parcels. Understanding and optimizing the optic characteristics of Zn-$Bi_2O_{3,}$nanocomposites are pivotal for maximizing their performance in practical operations. Hetero structure nanocomposite accoutrements have garnered exploration interest for their use in achieving precise control of material structures. Among numerous hetero structure nanocomposites, core-shell nanoparticles are composed of two or further types of accoutrements, in which one behaves as the ‘‘core’’ and the other acts as the ‘‘shell’’ (Liu et al., 2017). Accoutrements with miscellaneous core-shell nanostructures retain desirable parcels. Core-shell nanostructures enable the manipulation of distinctive or profitable physical and chemical parcels of the colorful chemical combinations to achieve enhanced electrochemical, optic, electrical and mechanical parcels (Yevtushenko et al., 2018). Styles for preparing core-shell- structured nanomaterials have attracted adding attention in recent times (Al et al., 2022). Composite systems of noble essence nanoparticles bedded in dielectric material matrices with high refractive indicator frequently parade large third-order optic nonlinearities and fast response time because of the improvement of the original field near and inside the essence patches around the face Plasmon resonance (SPR) (DADVSI et al., 2018). It has been attracting great amenities because of their essential operations in all-optic switches, optic correlates, phase conjugates and optic computing (Schlesinger metal., 2013). Recent advances in the figure-controlled conflation of colloidal core − shell nanoparticles allow for the forfeiture-tuning of the synergistic parcels of the patches through deliberate control over important geometric parameters, similar as the core shape, the shell infrastructures, the compositional arrangement, and the interfacial structures. Bismuth trioxide has lower poisonous, good conductivity, large energy band gap, and good photocatalyst exertion (Bulk et al., 2024).

$Bi_2O_{3,}$ is one excellent onto-electronic material, and it's also one of the effective factors of third-order nonlinear optic spectacles. It was reported that the nonlinear vulnerability of $Bi_2O_{3,}$ nanoparticles was 100 times larger than that of the bulk $Bi_2O_{3,}$ (Iqbal et al., 2017). Still, the microstructure of $Bi_2O_{3,}$ nanoparticles and their luminescent parcels were infrequently reported (Janeiro et al., 2014). In comparison to other noble essence counterparts, similar as Au, Pb, Pt, and Cu, Zn nanoparticles have far stronger Plasmon resonances, wider optic tuning range, more violent near- fi ELD advancements, and lesser refract metric Plasmon receptivity (Rahman et al., 2020). Zinc nanoparticle is frequently used as detectors because of its favorable optic parcels (Janeiro et al., 2015). Zn-$Bi_2O_{3,}$, is a considerably used emulsion of Bismuth, owing to its chemical stability, lower toxin, and its unique physical and chemical parcels. It's reported to have comparatively high ionic conductivity than other essence oxides and has made itself a feasible choice for colorful energy harvesting and seeing operations. (Barton et al., 2020). It also exhibits photocatalytic exertion which can be tuned and enhanced by incorporating certain accoutrements (Yasser et al., 2024). Zn-$Bi_2O_{3,}$nanocomposite is of interest recently due to their flawless medication as well as enhanced parcels furnishing prospects in photocatalysis, nanoscale optoelectronics and glamorous operations (CHO et al., 2016). Due to the noble parcels and operation of bismuth oxide and zinc patches, we studied theoretically and experimentally. As far as our knowledge concern, the compound of these accoutrements in experimental theoretical way isn't yet studied. In experimental system both chemical and green conflation route are incorporated for comparison. In recent times, green conflation of nanoparticle has attracted a great attention because of drug and natural operations. In this work, $Bi_2O_{3,}$ nanoparticle prepared via green conflation and chemical conflation routes. And we synthesized Zn-$Bi_2O_{3,}$nanocomposites using green conflation route. The synthesized nanoparticles were characterized using well given bias Pl and XRD. For theoretical styles we employ Mathematical Wolfram software to probe the optical properties of Zn-$Bi_2O_{3,}$nanocomposites through theoretical modeling and simulation. Using simulation, it can be delved how the optical properties of a core-shell nanoparticle evolve by changing the core compass and shell.

The paper is organized as follows: chapter one describes the introductory part of the thesis. In chapter two, we review some documents related to our work. In chapter three we discussed about materials and methods we used. Experimental and theoretical studies were discussed under methodology part chapter four. Finally, chapter five displays the conclusion and recommendation.

1.2 Statement of the Problem

In recent times, nanocomposites have surfaced as promising campaigners for colorful technological operations due to their unique parcels arising from the synergistic goods of their ingredients. Among these, Zn-$Bi_2O_{3,}$ nanocomposites have garnered significant attention owing to their implicit operations in optoelectronic bias, photovoltaics, and photocatalysis. still, despite their promising eventuality, there remains a critical gap in our understanding of their optic parcels, which hinders their effective application in practical operations. The gap in the study of optical properties of Zn-$Bi_2O_{3,}$ nanocomposites lie in the lack of comprehensive exploration fastening specifically on this material system. While there has been significant interest in nanocomposites for colorful operations, including optoelectronics, photovoltaics, and photocatalysis, the specific optical properties of Zn-$Bi_2O_{3,}$ nanocomposites remain unexplored.

1.3 Significance of the Study

The optical properties of Zn-$Bi_2O_{3,}$ nanocomposites play a pivotal part in their seeing capabilities. By studying these parcels, experimenters can develop largely sensitive and picky optic detectors for operations similar as environmental monitoring, biomedical diagnostics, and chemical seeing. Probing the optic parcels of Zn-$Bi_2O_{3,}$nanocomposites contribute to the broader field of accoutrements wisdom. It provides receptivity into the abecedarian principles governing light-matter relations at the nanoscale, easing the development of new accoutrements with acclimatized optic functionalities. And the experimenter can use this material for colorful fields.

1.4 Objective of the Study

1.4.1 General Objective

The general objective of this work was to study, synthesize and characterize Zn-$Bi_2O_{3,}$ nanocomposite using theoretical and experimental method.

1.4.2 Specific Objective

The specific objectives are:

- To study polarizability, refractive index and optical absorbance of Zn- $Bi_2O_{3,}$ nanocomposite.
- To investigate the effect of core size, shell thickness on optical response of Zn-Bi_2O_3 .
- To synthesize and characterize Zn-$Bi_2O_{3,}$ heterostructure nanocomposite.
- To compare the result of biological and chemical synthesis of Zn-$Bi_2O_{3,}$ nanocomposite.

CHAPTER TWO

Review of Related Literature

1 Bismuth Tri Oxide (Bi_2O_3) Nanoparticles

Bismuth tri oxide ($Bi_2O_{3,}$) fluently forms solid results with numerous other essence oxides. The chemistry of bismuth tri oxide is veritably intriguing exploration area in result and solid workshop. $Bi_2O_{3,}$is explosively polymorphic, α, β, γ, δ and ω forms are known. (Kumar et al., 2013). Phase diversity in bismuth tri oxide is precious area for doing different exploration in the base of phase metamorphosis in bismuth oxide base structure (Armored et al. 2015). $Bi_2O_{3,}$ Plays a significant part within the class of semiconducting oxide accoutrements, due to a variety of physical parcels determined by its multitudinous polymorphs (Though et al., 2016). This semiconductor is characterized by significant values of band gap, refractive index and dielectric permittivity, as well as remarkable photosensitivity and photoluminescence (Voter, et al., 2015). Depending on medication technology, which favors the ascendance of certain phases, its electrical conductivity may vary by over 5 orders of magnitude, while its energy gap may change from about 2 to3.96 eV (Janeiro et al., 2015). $Bi_2O_{3,}$is applicable for several operations in present solid-state technology. It’s extensively used in optoelectronics, optic coatings, as well as in transparent and superconductor ceramic glass manufacturing (EU et al., 2017).

2.2 Core- Shell Nanocomposite

Nanostructures are the structures, whose sizes are within nanometers (< 100 nm) and can comprise either single material or multiple material. Nanostructures with multiple material can again moreover be in the form of core – shell or simple like polymer – essence nanocomposite (DADVSI et al., 2018) At the same time, the core – shell nanocomposite can live in different sizes and different shapes like globular, centric, eccentric, star- suchlike, or tubular. For the former one, the shell with ineffective material can control the response rate by affecting the prolixity rate of reactants into the patches (Khan et al., 2019). The shell can also act as a defensive subcaste precluding the core material from high temperature, side- reactant or others that will affect the decay of the effective material. Likewise, in the pharmaceutical assiduity, industrialists can actually use the shell to maintain control of the releasing rate or releasing time for the core material for precise medical care (Barton, et al., 2020). Different types of cores- shell nanostructures can be designated with a variety of combination of parcels in mind similar as dielectric- essence, dielectric- semiconductor, essence- dielectric, semiconductor- essence, and numerous others. Core – shell structure can sustain the maximum face area for patches which have the effective material distributed in the shell (Gain et al., 2016). The participation of ineffective material as core can lower the consumption of effective material in each flyspeck (Yi et al. 2020).

The prolixity resistance is much lower than the flyspeck completely made of effective material, besides, with all the effective material in the shell covering the core (Liu et al., 2017). One of the advantages of core – shell nanostructures is to reduce the consumption of the precious material by sheeting the precious material with a provident material (EU et al. 2017). The high face area of metallic core structures yields high face powers, promoting face oxidation, and patches aggregation or clustering in physiological surroundings whereas shell material being carpeted over core material won't only inhibit the face oxidation but will also render stability again stag agglomeration. In numerous cases, coating has been set up to enhance the functionality as well (Kumar et al., 2016). The parcels of core – shell nanostructures arise from either core or shell or from both mates and hence are largely functional accoutrements. Likewise, by altering the constituting material and core to shell rate, the parcels can be changed. Still, consistence and structure of the shell may hamper the core parcels.

The core – shell assemblage should therefore be optimized according to the designed performance (Janeiro et al., 2015). Combining different new accoutrements in a single nanocomposite gain numerous amenities due to the fresh functionalities displayed. utmost is the globular nanocomposites are designed from noble essence similar Zinc (Zn) and semiconductor $Bi_2O_{3,}$accoutrements are a many exemplifications of similar compound nanoparticles. They can display exceptional physical and chemical parcels than individual patches, which set up a wide range of operations in nanotechnology (EU et al., 2017).

2.3 Model Core- Shell Nanocomposite

The core – shell structures are compound accoutrements that contain an inner core carpeted with one or more layers(shells) of different accoutrements. The accoutrements of the core – shell structures can live in different combinations, similar as core and shell accoutrements that are organic or inorganic (Arboleda et al., 2016). Likewise, organic cores can be carpeted with inorganic shells and vice versa. The physical and chemical parcels of core – shell nanoparticles are substantially associated with the accoutrements and structure of the core and shell, but they're also associated with the interface. This structure dependence provides huge openings and possibilities for manipulating parcels by controlling the chemical compositions and relative sizes of the core and shell (Chavez et al., 2017). The selection of the core and shell material is related to the type of targeted operation. Thus, the design of multifunctional core – shell nanoparticles generally depend on the final operation. For medicine delivery, the core material could retain glamorous characteristics, and the external shell could be a polymer or pervious silica (Bartoli et al., 2020).

2.4 Plasmonic Nanostructure

Plasmonic nanostructure is getting a seductive field due to its implicit operations in numerous areas. The plasmonic parcels of noble metallic can be tuned by changing the size and shape of both the core and the overall patches. With sweats from scientists in different areas, plasmonic nanostructures are used in the optic device, photonic circuits and detectors as well as in medical diagnostics. likewise, plasmonic nanostructures have met tremendous successes in nano electronics, chemistry, biology, drugs, catalysis, electro- catalysis, and in biomedical field. also, metallic fleece core- shell structures had been successfully introduced to passivate the face and tune the face plasmon resonance wavelength (Janaki et al., 2015).

2.4.1 Basic Idea of the Plasmonic Resonance

A snippet consists of a positive core girdled by an electron pall. Due to the commerce of the tittles with the incident radiation, the electrons in the conduction band are shifted consequent of the force wielded by the external electric field. The columbic commerce between the electrons and the protons acts as a restoring force which leads to electronic oscillations. These electronic collaborative oscillations of an essence are called Plasmon (Kumar et al., 2013). When one essence flyspeck is in an invariant electric field, the electron inside flyspeck moves from one side to the other side. also, the electrons will move back to the original position driven by the seductive force. As a result, the electrons will oscillate back and forth at a specific frequency, which is called tube frequency. And Plasmon is a quantization of these oscillation movements. Plasmon accoutrements have been playing a seductive part in the optic parcels of essence nanostructures. generally, essence is largely reflective accoutrements due to their tube frequency which lies in the ultraviolet diapason which is advanced than the frequency of visible light. The position and intensity of plasmon absorbance are largely affected by the face property of the accoutrements. For the face features including revision of plasmonic structure's shape, morphology and size, they could make different plasmonic modes (Cho et al, 2016).

2.4.2 Tunability of Plasmon Resonance

As we know optic parcels of the metallic nanoparticles depend explosively on the structural parameters (size and shape), type of the essence and the dielectric function of the girding material where they're bedded. Other parameters that have a dramatic effect on their optic response are the coupling between the plasmonic resonances in near structures, the exposure of the patches compare to the incident radiation, and the polarization state of the incident light (Chavez et al., 2017).

CHAPTER THREE

Materials and Methods

3.1 Materials

The materials and chemicals that were used for the thesis work are: furnace, oven, PH meter, thermometer, centrifuge, grinder, beaker, stirrer, distilled water, bismuth nitrate, zinc nitrate, ethanol and Whatman filter paper.

3.2 Experimental Methods

Nanoparticles or nanocomposites will synthesize in different method. The method we follow to synthesize our material is described as follow.

Synthesis of Bi_2O_3 Nanoparticle

To prepare Bi_2O_3 nanoparticles, 2 g of bismuth nitrate was dissolved in the 10 mL of distilled water and continuously stirred at 90 °C. also, the product washed several times with distilled water, and dry in a vacuum at 90 °C overnight. Also, the product was hooted at 550 °C in a furnace and stationary atmosphere of air for 5 h to insure the junking of contaminations (an unheroic greasepaint).

Green Synthesis of Bi_2O_3 Nanoparticle

First, Ruta graveolens leaves were gathered and washed completely with distilled water to remove the dust flyspeck. also, the leaves cut in to veritably fine pieces and dried. For the medication of splint excerpt, 10 g of the leaves of Ruta graveolens was immersed in 75 ml of distilled water and boiled at 90 °C for 2 hr. The attained splint excerpt was kept for cooling at room temperature, filtered using Whatman sludge paper. For the green conflation bismuth oxide nanoparticles, 2 g of bismuth nitrate was answered in the 10 mL of distilled water at 90 °C and mixed with 20 mL of waterless, Ruta graveolens excerpt at 90 °C under constant shifting for 24h. herbage conflation of Bi_2O_3 NPs was attained after 24 h at 90 °C. also, the product washed several times with double distilled water, and dry in a vacuum as the condition chemical conflation one. The product will be hotted at 550 °C in a furnace and stationary atmosphere of air for 5 h to insure the junking of contaminations (an unheroic greasepaint). The schematic response is as follow:

$$2BiNO_3 + \text{Ruta graveolens extract} \rightarrow Bi_2O_3$$

Green Synthesis of Zn-Bi_2O_3 Nanocomposite

To prepare Zn-Bi_2O_3 nanocomposite, 3.95 g Bi_2O_3 (as-synthesized) and 1.46 g Zn $(NO3)_3 5H_2O$ was dissolved in 75 mL ethanol and stirred at 70 ℃ for 1 h to achieve a transparent solution. Next 7.5 mL ethanol was added to the solution under vigorous stirring until a solution was obtained; the solution was then dried at 90 ℃ for 24 h. Finally, the sample is calcined at 500 ℃ for 2 h to obtain the Zn-Bi_2O_3 nanocomposite.

3.3 Numerical Method

Consider a spherical core- shell compound nanoparticle conforming of a semiconductor core of dielectric function(DF) ε_1 and a metallic shell of DF ε_2 bedded in a dielectric host matrix, as shown in Fig. 1. The host medium is assumed to be isotropic and non-absorbing with dielectric constant ε_3.

The parameters a_1 and a_2 are the diameters of the core and core- shell NP, independently. When an electromagnetic surge is incident on the compound core- shell NP, electric field is convinced in the system due to polarization. For NPs of sizes (diameter = $2a_2$) much lower than the wavelength of the incident light, the distribution of the electrostatic implicit Φ associated with the convinced field can be attained by working the Laplace equation, $\nabla_2\Phi = 0$ (Beyene et al, 2019).

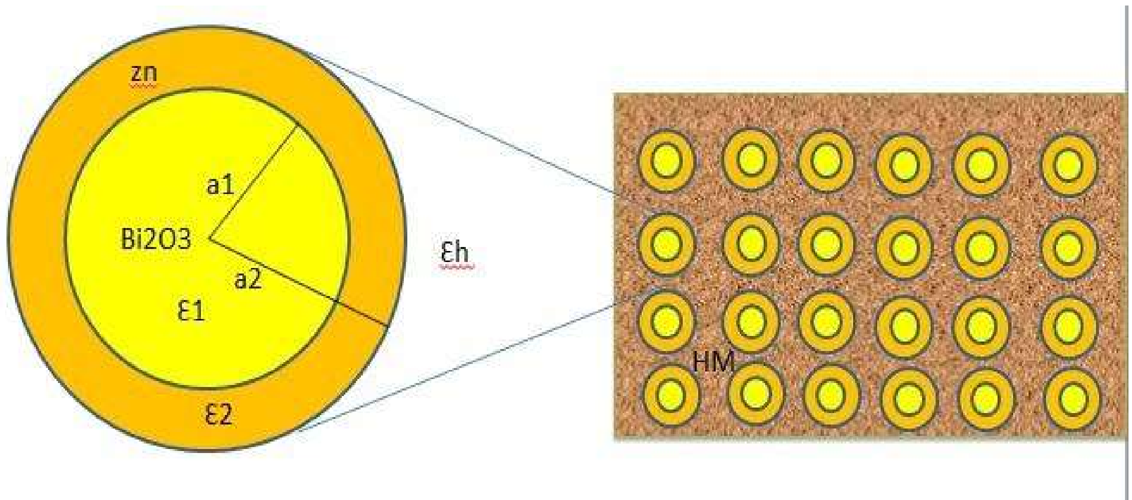

Figure 3.1: The schematic diagram of a core-shell spherical Nano inclusion embedded in host medium

Suppose a uniform stationary electromagnetic field concentrated along the z- axis is applied on the spherical core- shell NP bedded in a host matrix. However, also the distribution of the capabilities in the system may be set up to be If the center of the NP is assumed to coincide with the origin of a spherical coordinate system given by:

$$\Phi_1(r,\theta) = A_1 r cos\theta, \qquad r < a_1 \tag{3.1}$$

$$\Phi_2(r,\theta) = \left(A_2 r + \frac{B_1}{r^2}\right) cos\theta, \qquad a_1 < r < a_2 \tag{3.2}$$

$$\Phi_3(r,\theta) = \left(A_3 r + \frac{B_2}{r^2}\right) cos\theta, \qquad r > a_2 \tag{3.3}$$

where Φ_1, Φ_2, and Φ_3, are the potentials in the dielectric core, metal shell, and host matrix, respectively, A_3 is a quantity associated with the external applied field, r is the distance from the center of the NP, θ is the zenith angle, and the coefficients A_1, A_2, B_1, B_2 are constants to be determined by using the appropriate boundary conditions at the interfaces. Where the second term on the right-side of Eq. (3.3) represents the induced potential outside the core-shell NP. The optical properties of the system may readily have described by the induced field outside the concentric spheres. Consequently, it is sufficed to determine the value of the coefficient B_2. Imposing the relevant boundary conditions in equations.

$$B_2 = \left[\frac{(\varepsilon_1 + 2\varepsilon_2)(\varepsilon_2 - \varepsilon_h) + v_f(\varepsilon_1 - \varepsilon_2)(2\varepsilon_2 + \varepsilon_h)}{(\varepsilon_1 + 2\varepsilon_2)(\varepsilon_2 + 2\varepsilon_h) + 2v_f(\varepsilon_1 - \varepsilon_2)(\varepsilon_2 - \varepsilon_h)}\right] A_3 a_2^3. \tag{3.4}$$

In view of Eq. (3.3), the induced potential outside the concentric spheres is then given by

$$\Phi_{ind} = \left(\frac{B_2}{r^2}\right) cos\theta. \tag{3.5}$$

Moreover, employing the dipole approximation, induced potential may also be expressed as

$$\Phi_{ind} = \frac{pcos\theta}{4\pi\varepsilon_h r^2}, \tag{3.6}$$

where p is the magnitude of the electric dipole moment of the system. In view of Eq. (3.5) and (3.6), the dipole moment becomes

$$p = 4\pi\varepsilon_h B_2 = \varepsilon_h \alpha A_3, \tag{3.7}$$

where α is the polarizability of the composite given by

$$\alpha = 4\pi \left[\frac{(\varepsilon_1 + 2\varepsilon_2)(\varepsilon_2 - \varepsilon_h) + v_f(\varepsilon_1 - \varepsilon_2)(2\varepsilon_2 + \varepsilon_h)}{(\varepsilon_1 + 2\varepsilon_2)(\varepsilon_2 + 2\varepsilon_h) + 2v_f(\varepsilon_1 - \varepsilon_2)(\varepsilon_2 - \varepsilon_h)}\right] a_2^3, \tag{3.8}$$

Further, the polarizability of an equivalent sphere of effective DF ε_I embedded in a host matrix of DF ε_h can be expressed in form of the Clausius-Mossotti relation. That is,

$$\alpha = 4\pi a_2^3 \frac{\varepsilon_I - \varepsilon_h}{\varepsilon_I + 2\varepsilon_h}. \tag{3.9}$$

$$\varepsilon_I = \varepsilon_2 \frac{(\varepsilon_1 + 2\varepsilon_2) + 2(\varepsilon_1 - \varepsilon_2)v_f}{(\varepsilon_1 + 2\varepsilon_2) - (\varepsilon_1 - \varepsilon_2)v_f} \tag{3.10}$$

Introducing the volume fraction β of a spherical core-shell nanostructure by

$$\beta = 1 - v_f = 1 - \left(\frac{a_1}{a_2}\right)^3, \qquad (3.11)$$

the effective DF of Eq. (3.9), may be rewritten as

$$\varepsilon_I = \varepsilon_2 \frac{\varepsilon_1(3/\beta - 2) + 2\varepsilon_2}{\varepsilon_1 + \varepsilon_2(3/\beta - 1)v_f}. \qquad (3.12)$$

Next, we consider an ensemble where identical **s**pherical core-shell NPs (nano inclusions) are homogeneously dispersed in a continuous host matrix of DF, ε_h. The polarizability and effective permittivity of the system may be described by using the Clausius-Mossotti relation together with the Maxwell-Garnet mixing theory. If N denotes the density number of the inclusions in the system, then the polarizability expressed in terms of the permittivity becomes:

$$\frac{N\alpha}{3} = \frac{\varepsilon_{eff} - \varepsilon_h}{\varepsilon_{eff} + 2\varepsilon_h}, \qquad (3.13)$$

where ε_{eff} is the effective permittivity and α is the polarizability defined by Eq. (3.9). In addition, Eq. (3.9) may conveniently be rewritten as

$$\alpha = 4\pi r_2^3 \eta,$$

where η is the dimensionless polarizability defined by

$$\eta = \frac{\varepsilon_I - \varepsilon_h}{\varepsilon_I + 2\varepsilon_h}. \qquad (3.14)$$

Substituting Eq. (3.13) into (3.14) and rearranging, we find that

$$\eta = 1 - \frac{3}{2}\left[\frac{\varepsilon_2\varepsilon_3\left(\frac{3}{\beta}-1\right)+\varepsilon_1\varepsilon_h}{\varepsilon_2^2+\varepsilon_1\varepsilon_2\left(\frac{3}{2\beta}-1\right)+\varepsilon_2\varepsilon_h\left(\frac{3}{\beta}-1\right)+\varepsilon_1\varepsilon_h}\right]. \quad (3.15)$$

Furthermore, the effective permittivity of the ensemble may be obtained by substituting Eqn. (3.9) and (3.15) into Eqn. (3.14). That is,

$$\varepsilon_{eff} = \varepsilon_h\left(\frac{1+2\xi\eta}{1-\xi\eta}\right) \quad (3.16)$$

Here, ξ is the filling factor of the inclusions given by

$$\xi = N\frac{4\pi r_2^3}{3}. \quad (3.17)$$

It is worthwhile to note that Eqn. (3.16) and (3.17) are general expressions for any two-layered spherical core-shell nanocomposite that are embedded in a dielectrics host matrix, regardless of whether the core-shell composites are metals, magnetic material, semiconductors, dielectrics or a combination of different more than two dissimilar materials. (Afzal et al,2023).

For numerical evaluation, we considered an ensemble that consists of spherical Zn-Bi_2O_3, core-shell quantum dots distressed in Biwax (ε_h= 2.5). In the frequency domain of interest, we assumed that the DF of the Bi_2O_3, core to be a real constant that is independent of frequency (ε_1= 3.5). In addition, the DF of the Zincshell is chosen to be the modified Drude form that takes into account its nano-size. That is,

$$\varepsilon_2(\omega) = \varepsilon_\infty - \frac{\omega_p^2}{\omega[\omega+i\Gamma(l_e)]}, \quad (3.18)$$

where ε_∞ is the permittivity at high frequencies, ω_p is the plasma frequency, $\Gamma(le)$ is the size dependent electron collision frequency, and ω is the frequency of the incident radiation. The size dependent damping parameter for Zinc can be expressed as

$$\Gamma(l_e) = \Gamma_0 + A\frac{v_F}{l_e} \quad (3.19)$$

where $\Gamma_0 = 1.06 \times 10^{14}$ rad/s is the bulk damping constant which is associated with dissipative losses, $v_F = 1.38 \times 10^6$ m/s is the velocity of electrons at the Fermi level, and A is a constant that accounts for the details of the electron scattering processes at the interfaces . The quantity l_e is the electrons effective mean free path, which for a spherical NP of core radius a_1 and core/shell radius a_2 is given by

$$l_e = \frac{a_2}{2}\left[\left(1 - v_f^{1/3}\right)\left(1 - v_f^{2/3}\right)\right]^{1/3} \quad (3.20)$$

Further, separating Eq. (3.18) into real and imaginary, we have

$$\varepsilon_2(\omega) = \varepsilon'_2(\omega) + i\varepsilon''_2(\omega) \quad (3.21)$$

Where

$$\varepsilon'_2 = \varepsilon_\infty - \frac{1}{z^2 + p^2} \quad and \quad \varepsilon''_2 = \frac{1}{z(z^2 + \rho^2)} \quad (3.22)$$

With

$$z = \omega/\omega_p \qquad and \qquad \rho = \Gamma(l_e)/\ \omega_p$$

Using the above equation, we can determine very important and required properties of the composite.

Polarizability

Since the permittivity (ε_2) is complex, the electric polarizability is also a complex function of the frequency ω. That is,

$$\eta = \eta' + i\eta'' \qquad (3.23)$$

where η' is the real part and η'' is the imaginary part. Substituting Eq. (3.18) into (3.15), we obtain

$$\eta' = 1 - \frac{3}{2}\left[\frac{(\varepsilon'_2\Delta_1 + \varepsilon_1\varepsilon_h)\gamma + (\varepsilon''_2\Delta_1)\delta}{\gamma^2 + \delta^2}\right] \qquad (3.24)$$

And

$$\eta'' = \frac{3}{2}\left[\frac{(\varepsilon'_2\Delta_1 + \varepsilon_1\varepsilon_h)\delta - (\varepsilon''_2\Delta_1)\gamma}{\gamma^2 + \delta^2}\right] \qquad (3.25)$$

Where

$$\Delta_1 = \varepsilon_h\left(\frac{3}{\beta} - 1\right),$$

$$\gamma = (\varepsilon'_2)^2 - (\varepsilon''_2)^2 + \varepsilon'_2\Delta_2 + \varepsilon_1\varepsilon_h,$$

$$\delta = 2\varepsilon'_2\varepsilon''_2 + \varepsilon''_2\Delta_2,$$

$$\Delta_2 = \Delta_1 + \varepsilon_1\left(\frac{3}{2\beta} - 1\right)$$

Below, the real and imaginary parts of the polarizability of the Zn- Bi_2O_3 core-shell NPs embedded in biwax are analyzed using Eqns. (3.24) and (3.25). The parameter values used for the numerical simulations are: ε_1 =3.5, ε_∞ = 3.5, ω_p = 1.03×10^{16} rad/s , γ_0 = 1.177×10^{14} rad/s V_f=1.38×10^{6} m/s, and A = 1

Refractive Index

The response of a medium to an incident electromagnetic wave may be described by

$$\tilde{n} = \sqrt{\varepsilon_{eff}} \qquad (3.26)$$

Where $\varepsilon_{eff} = \varepsilon'_{eff} + \varepsilon''_{eff}$ is the complex effective DF of the medium. Introducing the real (n) and imaginary parts (k), $\tilde{n}$ may be written as

$$\tilde{n} = n + ik \qquad (3.27)$$

Further, manipulating Eq. (3.27) together with ε_{eff} , we find that

$$\tilde{n}^2 = n^2 - k^2 + 2ikn = \varepsilon'_{eff} + i\varepsilon''_{eff} \qquad (3.28)$$

Hence, the real and imaginary parts of the refractive index, respectively, take the form:

$$n = \frac{1}{\sqrt{2}}\left[\left(\varepsilon'^2_{eff} + \varepsilon''^2_{eff}\right)^{1/2} + \varepsilon'_{eff}\right]^{1/2} \qquad (3.29)$$

$$k = \frac{1}{\sqrt{2}}\left[\left(\varepsilon'^2_{eff} + \varepsilon''^2_{eff}\right)^{1/2} - \varepsilon'_{eff}\right]^{1/2} \qquad (3.30)$$

CHAPTER FOUR

Result and Discussion

4.1 Numerical Analysis

4.1.1 Polarizability

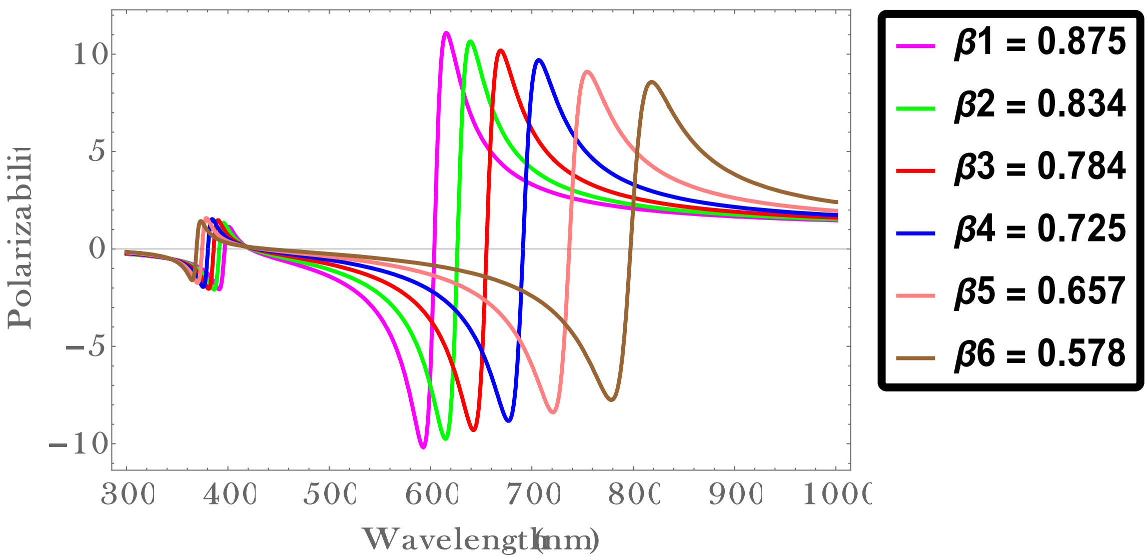

Figure 4.1: The real part of the polarizability of the spherical nanoinclustion as a function of wavelength for different values of β.

Figure4.1 Shows, the real part of the polarizability of the nanoinclusions as a function of the wavelength of the incident radiation for different values of volume bit, β. It's observed that the real part of the polarizability has two sets of resonances in the UV spectral region around λ = 300 nm and in the visible region above λ = 600 nm. The two sets of resonance peaks do as a result of the face Plasmon resonances of at the inner and external ($Zn\text{-}Bi_2O_3$, and (host matrix) interfaces. when the value of β is increased, which may be realized either by dwindling the size of the core or adding the consistence of the shell. When the core material attention is increased or the value of volume bit is increased, the two resonances are close each other and the alternate peak is more enhanced.

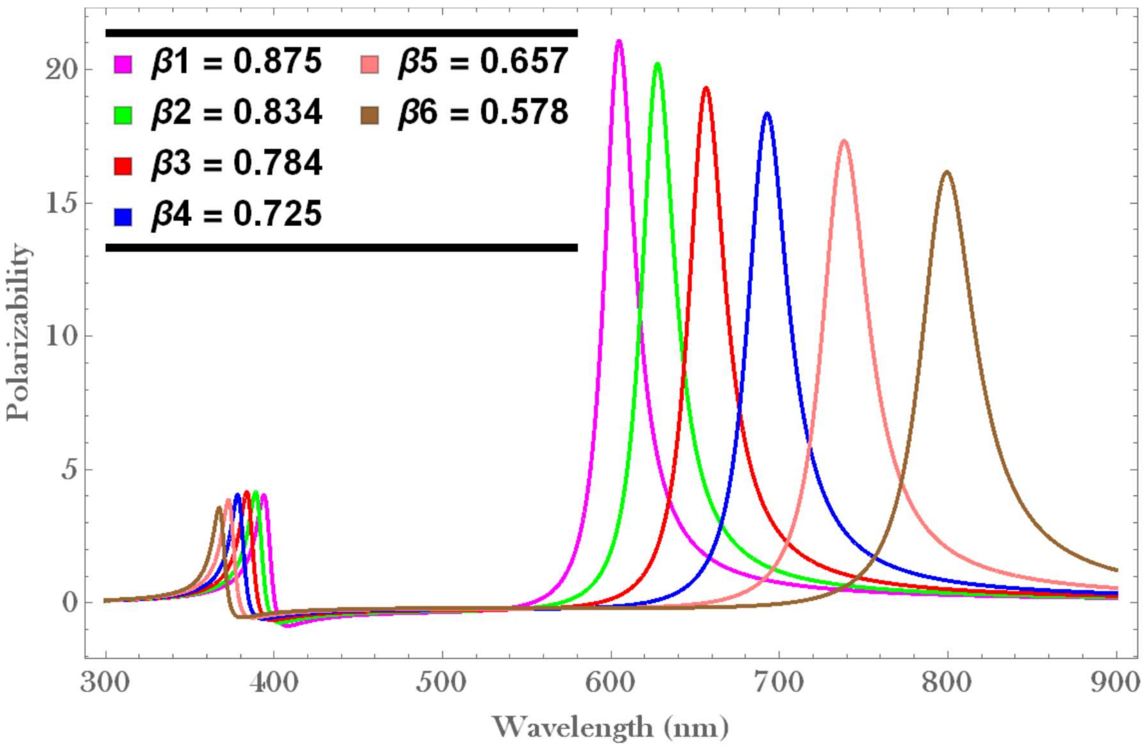

Figure 4.2: The imaginary part of the polarizability of the nanoinclusions obtained for different value of β.

Figure 4.2 shows that, the imaginary part of the polarizability of the Nano inclusions as a function of wavelength for different values of β. The two sets of resonance peaks are observed in the visible and near infrared regions. We used six (6) different values of β. For = 0.875, the first peak is located in the visible region at the wavelength λ = 400nm, whereas the alternate resonance peak is at λ = 550 nm in the visible and near infrared spectral region. From imaginary and real part of polarizability graph we conclude that as the essence consistence is increased the scattering of electrons at the interface from essence face to the dielectrics and the transmission of electrons in the essence came maximum.

4.1.2 Refractive Index

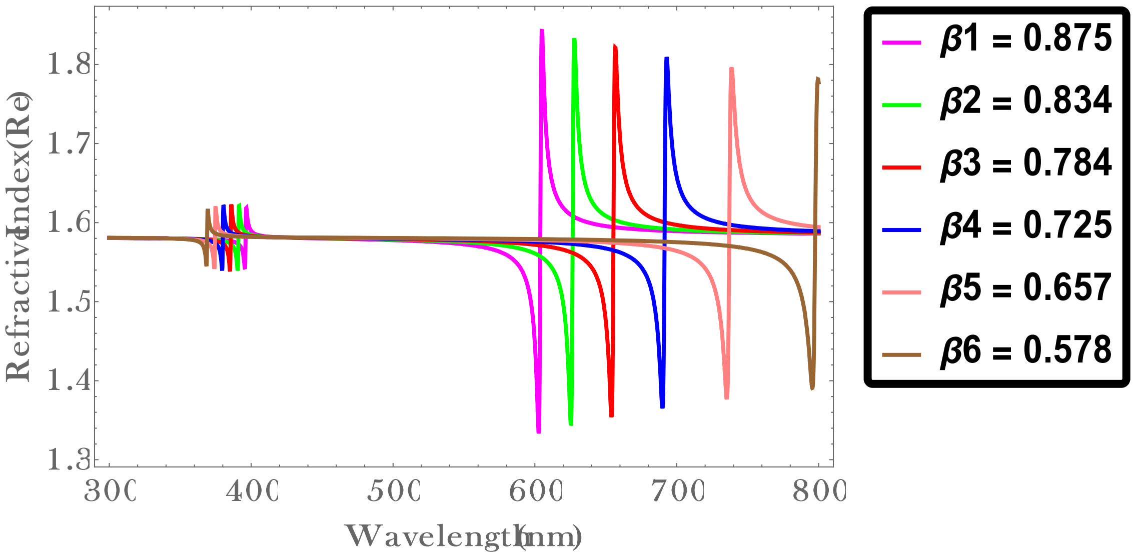

Figure 4.3: The real part of the refractive index as a function of wavelength for fixed filling factor ξ = 0.001and different values of β.

Figure 4.3 shows, the real part of refractive index as a function of wavelength of the incident light for afixed value of the filling factor ξ=0.001 and six different values of β. The graph indicates that the refractive index varies between 1.6 and 1.8 and possesses two sets of resonances corresponding to two anomalous dispersion regions; the first set in the visible region around 400 nm and the second peaks in the near infrared region between 600 nm. The peaks show slight red shifts in the visible region when the volume fraction, β is increased.

Figure 4.3 shows, the real part of refractive index as a function of wavelength of the incident light for a fixed value of the filling factor ξ = 0.001 and six different values of β. The graph indicates that the refractive index varies between 1.6 and 1.8 and possesses two sets of resonances corresponding to two anomalous dissipation regions; the first set in the visible region around 400 nm and the alternate peaks in the near infrared region between 600 nm. The peaks show slight red shifts in the visible region when the volume bit, β is increased

For the same parameters, the imaginary part of the refractive index is shown in Figure 4.4. As shown in the figure, 4.4 the figure has two resonance anomaly dispersions of the system. When the volume fractions of the concentric spheres are nearly unity, the imaginary part of the refractive index in the UV region is maximum. For six β values we seen that six different colors in the visible range to distinguish the response. Values of the maxima strongly depend on β.

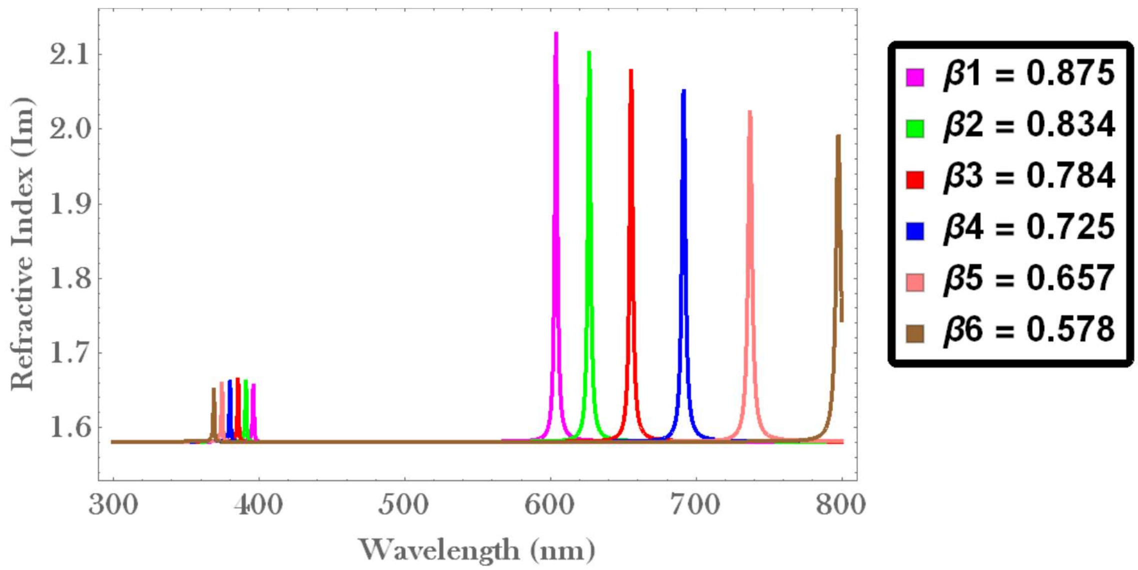

Figure 4.4: The imaginary part of the refractive index of the spherical inclusions obtained for different values of β and a fixed filling factor, ξ = 0.001.

It is clear to see that the optical properties of the Zn- Bi_2O_3 presented by the spectra of optical constant are significantly different from those of pure Zn and bismuth trioxide materials. Therefore, the optical properties can be carefully controlled and adjusted by changing the Zn concentration to satisfy the optical requirement in application.

4.1.3 Optical Absorbance

The spherical inclusions in the ensemble are polarizable, with field-induced dipoles, due to the interaction of the dipole moments with the applied uniform electric field. In our case, the incident field is assumed to be polarizable along the z-axis, and hence may be expressed as $E =$

$E_0 e^{[i\omega(\tilde{n}z-ct)/c]}$, where E_0 is the amplitude of the field, $\tilde{n}$ is the complex refractive index, and c is the speed of light in vacuum. Because of the presence of the term $e^{(-k\omega z/c)}$, the wave decays as it propagates in the composite nanostructure. An incident light, in general, propagating in a medium is attenuated both by absorption and scattering (Serhan et al, 2019, Shivola, 2000). However, for NPs that are much smaller than the wavelength of light, scattering effects may be neglected so that only the absorption contributes significantly to the attenuation. The intensity (I) of the propagating wave is related to the electric field by $I \sim |E|^2$. Generally, as the wave traverses in the medium, the intensity is attenuated as:

$$I = I_0 e^{-\alpha z} \tag{4.1}$$

Where I_0 is the intensity at z = 0 and α is the absorption coefficient defined by

$$\alpha = \frac{2k\omega}{c} = \frac{4\pi k}{\lambda}, \tag{4.2}$$

where $\lambda = 2\pi c/\omega$ is the wavelength of the incident radiation and k is the imaginary part of the refractive index. The typical length of light propagation in a material medium is represented by the absorption length l, which is defined by $l = 1/\alpha$. The quantity in the exponent of Eq. (4.14) is the absorbance (A) which may generally be expressed as $A = \ln(I_0/I_t) = t\alpha$, where I_t is the intensity at z = t. Thus, for the Zn@ Bi_2O_3 nanocomposites, the absorbance at the inner interface is given by:

$$A(\lambda) = \frac{2k\omega}{c} t_{Zn} = \frac{4\pi k}{\lambda} t_{Zn}, \tag{4.3}$$

where $t_{Zn} = a_2 - a_1$ is the thickness of the Zn shell. Figure 4.5 depicts the absorbance of the spherical Zn@Bi_2O_3 nano inclusions as a function of wavelength for $\xi = 0.001$ and different values of β (or t_{Zn}); while the core-shell radius (20 nm) is kept constant. It shows two sets of absorption peaks: the first and the second are in the visible and near infrared spectral regions, respectively.

The spherical inclusions in the ensemble are polarizable, with field-induced dipoles, due to the interaction of the dipole moments with the applied uniform electric field. The surface plasma resonance effect of Zn shell leads the absorption peaks to be found in the 500–600-nm wavelength range. The intensity of the resonant peak increases with the position shifted toward the long wavelength as the Zn thickness increases. The shift can be attributed to the increasing electromagnetic interaction between metal particles with the change of the effective permittivity.

Figure 4.5 illustrates how the face Plasmon resonance shifted to an advanced wavelength (red shift) due to the increased Zn NPs. Due to the lower distribution of the core – shell nanoparticles, the bands widen with adding Zn NP. It's the conformation of Zn on the face of Bi2O3 that causes the change in face Plasmon adsorption, which implies the successful production of core – shell Zn-Bi_2O_3 nanoparticles.

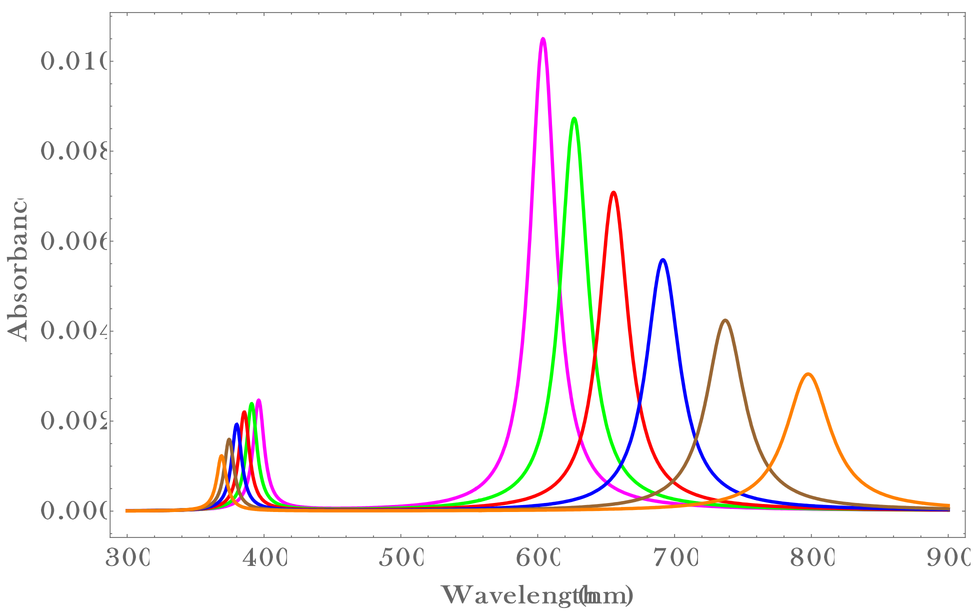

Figure 4.5: The absorbance of the nanoinclusions obtained for different values of t_{Zn} and ξ=0.001. The radii of the QDs is a_2=20nm

4.2. Experimental Analysis

4.2.1 Photoluminescence (PL) Analysis

i. PL analysis for Bi_2O_3 nanoparticles

From PL result of Bi_2O_3 nanoparticles, the peak is observed at 528 nm in the range 520 -540 nm region as shown in fig 4.6 below. The band gap (Eg) was calculated by using the experimental data which is Eg = 2.41 eV.

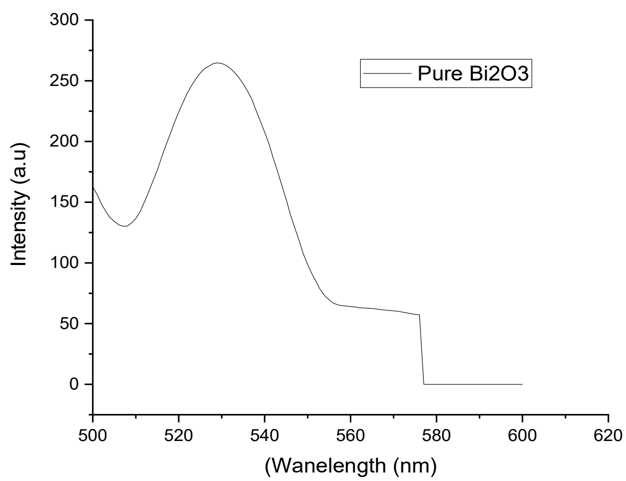

Figure 4.6: PL of Bi_2O_3 nanoparticles

ii. PL analysis for Bi_2O_3 nanoparticles with green synthesis

From PL result of Bi_2O_3 nanoparticles using green synthesis method, the peak is observed at 530 nm in the range 500 -550 nm region. By using experimental data, we calculate the band gap Eg = 1.39 eV. Comparing the result of pure Bi_2O_3 with the green synthesis method, the band gap for the green synthesis is lower than the pure one. And there is phase shift from both results. From this result, green (biological) synthesis route has a great role on the crystallite of the material. The materials synthesized using the green one can used to photosynthesis. The application and synthesize procedure is friendly interact with the environment.

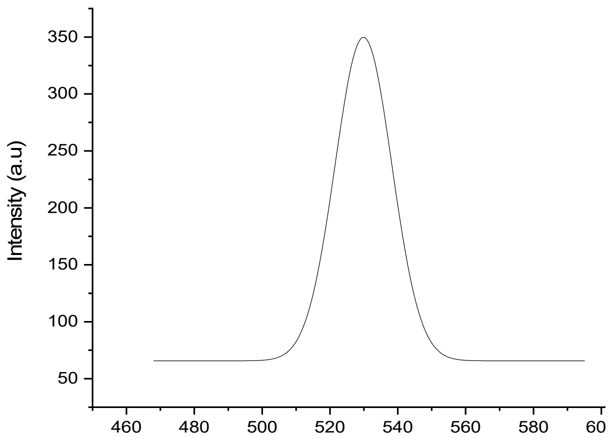

Figure 4.7: Pl of Bi_2O_3 nanoparticles using green synthesis method

iii. PL analysis for Zn-Bi_2O_3 Nanocomposite using green synthesis method

From PL result of $Zn - Bi_2O_3$ nanocomposite with green the peak is observed at 530 nm in the range 520 -540 nm region. The band gap was calculated using experimental data, Eg = 2.21 eV. When Bi_2O_3 combine with metal Zn, its properties are changed. As we seen from the graph, the peak intensity and position is changed and the application will have changed too. The application of a certain materials depends on their properties.

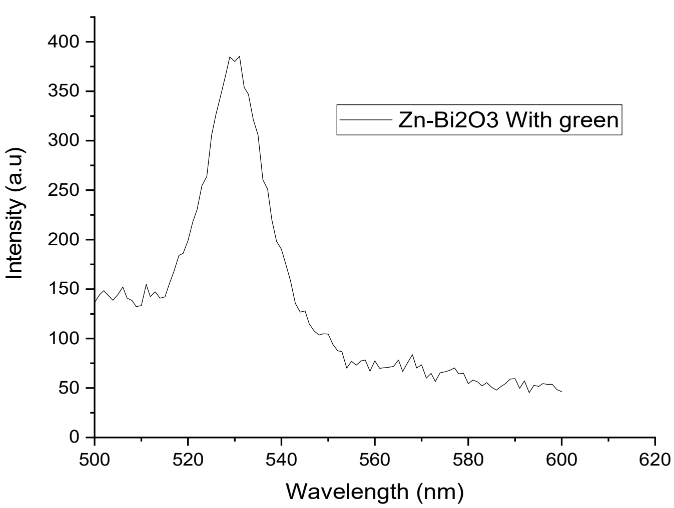

Figure 4.8: PL of Zn-Bi_2O_3 nanocomposite using green synthesis route

4.2.2 XRD Analysis

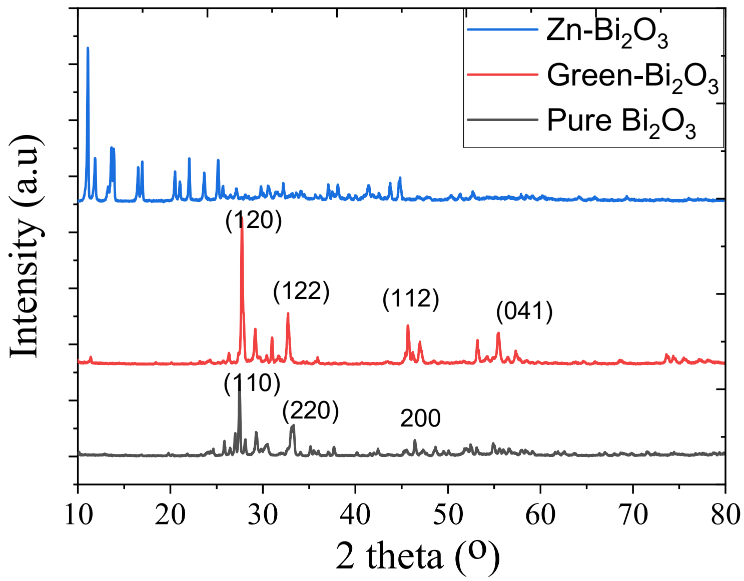

Figure 3.9: XRD graph of Bi_2O_3 nanoparticles and Zn-Bi_2O_3 nanocomposite.

The XRD result shows that for pure Bi_2O_3 and Bi_2O_3 with ruta graveolens the peaks are appeared that are anticipated. The peaks showed well-align of the material with crystalline peaks at (110) plane for pure Bi_2O_3 and at (120) plane. The Bi_2O_3 patterns vindicated that the crystal structure was successfully formed. Grounded on the exposure at the (120) plane, the synthesized material showed prominent peaks. The most conspicuous peaks, with strong exposure on the (120) plane, were recorded by Bi_2O_3 with ruta graveolens.This result is analogous to the former reported pattern.

Comparing with Zn- with green conflation one, there are numerous peaks. These number of peaks arise due to impurity occurs during our experimental work. Due to infinitesimal rearrangement, some peaks' intensity is reducing and lowered. Due to the modest ionic size of zinc, the addition of zinc doesn't significantly alter the crystal clear structure thus; there's no perceptible peaks shift. In all cases, the sizes of materials are in nanoscale.

CHAPTER FIVE

Conclusion and Recommendation

The nanoparticle was prepared by green synthesis using ruta graveolens as reducing agent. Also it was synthesized without green conflation system. The composite of metal zinc and Bi_2O_3 is also synthesis using biological synthesis route. The synthesized accoutrements were characterizing by using Pl and XRD spectroscopy. By using our experimental data, we calculate the bandgap for each. The result shows the bandgap for the green synthesis is lower than the pure one. The XRD result shows that the Bi_2O_3 patterns vindicated that the crystal structure was successfully formed. Grounded on the exposure at the (120) plane, the synthesized material showed prominent peaks. The most conspicuous peaks, with strong exposure on the (120) plane, were recorded by Bi_2O_3 with ruta graveolens. The numerical study shows that for different values of essence bit and filling factor, the polarizability, refractive indicator, and optical absorbance of the ensemble parade two set of resonance peaks in the visible and visible-near infrared (between $550 - 600$ nm) spectral regions. These peaks are attributed to the face Plasmon resonance of at the Zn- and Zn/ host- matrix interface. also, when the Zn shell consistence is increased, the observed resonance peaks are enhanced. Using simulation, we delved how the optic parcels of a core- shell nanoparticle evolve by changing the core compass and shell consistence parameters. The core- shell structured Zn- nanocomposite displayed considerable immersion and refraction which are similar to the Zn NPs.

The observed strong saturated absorption behavior suggested that the Zn-Bi_2O_3 core-shell NPs and other form of composite could be a potential material for optical limiting applications and environmental remediation. Therefore; future works can focus on utilizing the findings of this study to develop and optimize such devices.

References

Abdaalameer, N. K., Mazhir, S. N., & Aadim, K. A. (2021). Diagnostics of zinc selenite plasma produced by FHG of a Q-switchedND: YAGlaser. *Chalcogenide Letters*, *18*(7), 405-411.

Afzal, S., Tehreem, S., Munir, T., Sarwar, S. G., & Ikhioya, L. I. (2023). Impact of Transition Metal Doped Bismuth Oxide Nanocomposites on the Bandgap Energy for Photoanode Application. *Journal of Nano and Materials Science Research*, *2*(1), 104-109.

Al-Buriahi, M. S., Hessien, M., Alresheedi, F., Al-Baradi, A. M., Alrowaili, Z. A., Kebaili, I., & Olarinoye, I. O. (2022). ZnO–Bi2O3 nanopowders: Fabrication, structural, optical, and radiation shielding properties. *Ceramics International*, *48*(3), 3464-3472.

Arboleda, D. M., Santillán, J. M., Herrera, L. J. M., Muraca, D., Schinca, D. C., & Scaffardi, L. B. (2016). Size-dependent complex dielectric function of Ni, Mo, W, Pb, Zn and Na nanoparticles. Application to sizing. *Journal of Physics D: Applied Physics*, *49*(7), 075302.

Bartoli, M., Jagdale, P., & Tagliaferro, A. (2020). A short review on biomedical applications of nanostructured bismuth oxide and related nanomaterials. *Materials*, *13*(22), 5234.

Beyene, G., Senbeta, T., & Mesfin, B. (2019). Size dependent optical properties of ZnO@ Ag core/shell nanostructures. *Chinese Journal of Physics*, *58*, 235-243.

Chavez, F. A., & Srinivasan, G. (2017). Self-assembly of nanostructures with multiferroic components using nucleic acid linkers. *MRS Communications*, *7*(1), 20-26.

Dadashi, S., Poursalehi, R., & Delavari, H. (2018). Optical and structural properties of oxidation resistant colloidal bismuth/gold nanocomposite: An efficient nanoparticles based contrast agent for X-ray computed tomography. *Journal of Molecular Liquids*, *254*, 12-19.

Ibrahim Khan, K. S., & Khan, I. (2017). Nanoparticles: Properties, applications and toxicities. *Arabian journal of chemistry*, *12*(7), 908-931.

Ievtushenko, A., Karpyna, V., Eriksson, J., Tsiaoussis, I., Shtepliuk, I., Lashkarev, G., ... & Khranovskyy, V. (2018). Effect of Ag doping on the structural, electrical and optical properties of ZnO grown by MOCVD at different substrate temperatures. *Superlattices and Microstructures*, *117*, 121-131.

Iqbal, A., & Shamim, U. (2024). Synthesis of Zn/Bi2O3 composite for photodegradation of dyes in aqueous medium and its characterization.

Janaki, A. C., Sailatha, E., & Gunasekaran, S. (2015). Synthesis, characteristics and antimicrobial activity of ZnO nanoparticles. *Spectrochimica Acta Part A: Molecular and Biomolecular Spectroscopy*, *144*, 17-22.

Kayani, Z. N., Manzoor, F., Zafar, A., Mahmood, M., Rasheed, M., & Anwar, M. (2020). Impact of Ag doping on structural, optical, morphological, optical and photoluminescent properties of ZnO nanoparticles. *Optical and Quantum Electronics*, *52*, 1-18.

Kholghy, M. R., Veshkini, A., & Thomson, M. J. (2016). The core–shell internal nanostructure of soot–A criterion to model soot maturity. *Carbon*, *100*, 508-536.

Kumar, S. S., Venkateswarlu, P., Rao, V. R., & Rao, G. N. (2013). Synthesis, characterization and optical properties of zinc oxide nanoparticles. *International Nano Letters*, *3*, 1-6.

Kumar, S., Singh, V., & Tanwar, A. (2016). Structural, morphological, optical and photocatalytic properties of Ag-doped ZnO nanoparticles. *Journal of Materials Science: Materials in Electronics*, *27*, 2166-2173.

Liu, D., Zhang, H., Cito, S., Fan, J., Mäkilä, E., Salonen, J., & Santos, H. A. (2017). Core/shell nanocomposites produced by superfast sequential microfluidic nanoprecipitation. *Nano letters*, *17*(2), 606-614.

Rahman, D. S., & Ghosh, S. K. (2016). Manipulating electron transfer in hybrid ZnO–Au nanostructures: size of gold matters. *The Journal of Physical Chemistry C*, *120*(27), 14906-14917.

Schlesinger, M., Schulze, S., Hietschold, M., & Mehring, M. (2013). Metastable β-Bi_2O_3nanoparticles with high photocatalytic activity from polynuclear bismuth oxido clusters. *Dalton transactions*, *42*(4), 1047-1056.

Schwarz, C. M., Kang, M., Altemose, Q., Raichle, K., Schnable, B., Grabill, C., ... & Kuebler, S. M. (2020). Processing and properties of novel ZnO–Bi2O3–B2O3 glass-ceramic nanocomposites. *Journal of Alloys and Compounds*, *820*, 153173.

Serhan, M., Sprowls, M., Jackemeyer, D., Long, M., Perez, I. D., Maret, W., Tao, N., & Forzani, E. (2019). Total iron measurement in human serum with a smartphone. *AIChE Annual Meeting, Conference Proceedings*, *2019-Novem*. https://doi.org/10.1039/x0xx00000x

Shivola, A. (2000). Mixing rules with complex dielectric coefficients. l. Appl. 1 (4):393–415. doi: 10.1023/A:1026511515005. *Subsurf. Sens. Technol. Appl.*, *1*(4), 393–415.

Simeyon, V., Dinesh, A., Deivatamil, D., Thiruneelakandan, R., Meena, B. C., Mathavi, M., ... & Fouad, H. (2024). Bi2O3/ZnO heterostructured semiconductor nanocomposites: synthesis, characterization and its visible light-induced degradation of methylene blue dye. *Zeitschrift für Physikalische Chemie*, *238*(3), 421-435.

Viter, R., Balevicius, Z., Abou Chaaya, A., Baleviciute, I., Tumenas, S., Mikoliunaite, L., ... & Bechelany, M. (2015). The influence of localized plasmons on the optical properties of Au/ZnO nanostructures. *Journal of Materials Chemistry C*, *3*(26), 6815-6821.

Xu, L., Zheng, G., Liu, Y., Su, J., Kuang, W., & Rao, W. (2017). The optical properties of Ag/ZnO nanocomposite thin films with different thickness. *Optik*, *147*, 6-13.

Yasser, H. K., Aldhuhaibat, M. J., & Farhan, A. J. (2024, February). Investigation of mechanical and radiative attenuation traits of PMMA/ZnO/Bi2O3 hybrid nanocomposites. In *AIP Conference Proceedings* (Vol. 2922, No. 1). AIP Publishing.

Yi, W. Y., Yang, Y. H., Li, J. L., & Yang, G. W. (2020). Tunable emission in ZnO/Bi2O3 nanocomposites. *Materials Letters*, *277*, 128326.